J. Membrane Biol. 47, 39–57 (1979)

Limitations of the Eadie-Hofstee Plot to Estimate Kinetic Parameters of Intestinal Transport in the Presence of an Unstirred Water Layer

Alan B.R. Thomson

Department of Medicine, 9-112 Clinical Sciences Building, University of Alberta, Edmonton, Alberta T6G2G3

Received 3 August 1978; revised 28 December 1978

Summary. In the presence of an intestinal unstirred water layer, the relationship between substrate concentration (C_1) and unidirectional flux (J_d) is not described by the equation for a rectangular hyperbole. Accordingly, transformations of the Michaelis-Menten equation may not necessarily be linear and may lead to serious errors in the estimation of the affinity constant (K_m) and maximal transport rate (J_d^m) of carrier-mediated processes. An equation has previously been derived which described J_d under conditions of varying effective thickness or surface area of the unstirred water layer, the free diffusion coefficient of the probe molecule, and the distribution of transport sites along the villus. These theoretical curves have been analyzed by using the Eadie-Hofstee transformation (J_d *vs.* J_d/C_1) of the Michaelis-Menten equation. Use of this plot leads to serious discrepancies between the true and apparent affinity constants and between true and apparent maximal transport rates. These differences are further magnified by failure to correct for the contribution of passive permeation. The Eadie-Hofstee plot is of use, however, to infer certain qualitative characteristics of active transport processes, such as the variation in affinity constants and overlying resistance of the unstirred water layer at different sites along the villus and to predict the adequacy of the correction for the contribution of passive permeation.

Experimental data of intestinal transport are often analyzed with a view of determining firstly whether they conform to Michaelis-Menten kinetics, and secondly what values may be obtained for the kinetic constants. I wish to consider graphical means by which it is possible to determine the maximal transport rate, J_d^m, and the affinity constant, K_m. This error is derived from two major considerations, failure to correct for the effect of the unstirred water layer and failure to correct for the contribution of the passive component which proceeds concurrently with carrier-mediated absorption. Since the equations describing active or carrier-mediated transport in the presence of significant unstirred layer resistance do not take the form of a rectangular hyperbole [15], it is

0022-2631/79/0047-0039/$03.80

incorrect to apply the Lineweaver-Burk plot to estimate the values of K_m and J_d^m. For the same reasons there may be limitations in the use of the Eadie-Hofstee derivation of the Michaelis-Menten equation. The effective resistance of the intestinal unstirred water layer is determined by the thickness and surface area of the unstirred layer, as well as by the free diffusion coefficient of the probe molecule [17, 12]. This resistance may be of sufficient magnitude to distort the linear relationship which would otherwise prevail when using the Eadie-Hofstee transformation [1] of the Michaelis-Menten equation.

Since it is the concentration of the substrate at the aqueous-membrane interface which determines the rate of uptake and since this value may differ significantly from the bulk phase concentration [12], then it is likely that the Eadie-Hofstee plot is not linear in the presence of unstirred layer resistance of the magnitude observed in the intestine.

On the other hand, the nature of the deviation from linearity may provide a theoretical basis for the formulation of certain possible qualitative characteristics of the transport process. For example, the distribution of the transport sites along the villus might produce a different qualitative relationship when the sites are located primarily near the tip of the villus, rather than when distributed evenly from villus tip to crypt. Accordingly, the present study was undertaken to determine the limitations of the Eadie-Hofstee derivation of the Michaelis-Menten equation in the estimation of the kinetic constants of intestinal carrier-mediated transport in the presence of an unstirred water layer; and secondly, to establish whether this plot might provide further insight into the nature of the intestinal transport process itself.

Method

If the effect of the unstirred water layer is negligible, and if the appropriate correction for the contribution of diffusion to the total measured values of unidirectional flux has been made, then carrier-mediated transport may be described by an equation for a rectangular hyperbole

$$J = \frac{J^m C_2}{C_2 + K_m} \tag{1}$$

where J is the rate of unidirectional flux, J^m is the maximal transport rate, C_2 is the concentration of the probe molecule at the brush border membrane, and K_m is the true

[1] The rate of uptake J_d is plotted against the rate of uptake divided by the concentration of the substrate C_1 in the bulk phase (J_d *vs.* J_d/C_1).

affinity constant of the carrier. While many previous studies of intestinal transport have described a curvilinear relationship between substrate concentration and absorption, a plateau is rarely achieved, and it may accordingly be difficult to accurately assess J^m and therefore K_m. To overcome this difficulty, Eq.(1) is often rearranged to conform to a straight line. There are three possible linear transformations of this equation, each of which has its own limitations and errors. The use of the Lineweaver-Burk double reciprocal plot may be associated with errors in the estimation of the maximal transport rate and the affinity constant [15]. This presentation will consider the Eadie-Hofstee transformation of the Michaelis-Menten equation. Equation (1) may be written in a linear form by multiplying by (C_2+K_m) and rearranging

$$J=J^m-\frac{J\cdot K_m}{C_2}. \tag{2}$$

Since J^m and K_m are constant for a given process, J is proportional to J/C_2 and the relationship between J *vs.* J/C_2 is linear, with a slope of $-K_m$ and a y-axis intercept of J^m. The K_m can be derived from the slope $(-K_m)$; alternatively K_m can be calculated from the value of the x-axis intercept J/C_2, in which case J^m is substituted for J and K_m is solved. It is apparent from this consideration, however, that any error in the estimate of either K_m or J_d^m will significantly influence the estimate of the magnitude of the other.

The concentration term in Eq.(2), C_2, is the concentration of the probe molecule at the aqueous membrane interface. As a result of the effective resistance of the unstirred water layer [12], this value is equal to or less than the concentration of the probe molecule in the bulk phase, as given in Eq. 3

$$C_2=C_1-J(d/D). \tag{3}$$

In addition, Eq. (2) cannot be utilized for intestinal transport work since the units of the flux term, J in this formulation must be mass time$^{-1}\cdot$unit surface area^{-1} and, furthermore, the surface area of the unstirred layer must equal that of the underlying membrane. Because of the complexity of the intestinal mucosa with both villi and microvilli, uptake rates are commonly normalized to some parameter such as dry wt of tissue that is assumed to bear a constant relationship to the surface area of the functional membrane through which active transport occurs. We have designated such experimentally determined flux rates as J_d and normalized them to 100 mg dry wt of intestine so that our observed rates of active solute transport have the units nmol/100 mg$^{-1}\cdot$min^{-1} [5, 9, 12, 14]. In order to correct for unstirred layer resistance, it is necessary to know the effective surface area of the diffusion barrier through which the observed flux of solute, J_d took place. We have designated this term S_w and it has the units cm$^2\cdot$100 mg^{-1}. Thus J_d/S_w equals J, J_d^m/S_w equals J^m and C_2 equals $C_1-J_d(d/S_wD)$.

A new equation has previously been derived to describe the relationship between the experimentally determined unidirectional flux rate J_d and the concentration of the probe molecule in the bulk phase, C_1, in the presence of varying effective thickness d and surface area S_w of the unstirred layer, for a probe molecule with a diffusion coefficient D, for a carrier with a maximal transport rate J_d^m and true Michaelis affinity constant of K_m, with the proportion of the maximal transport occurring at an n-th villus site designated as f_n [10]. This equation is

$$J_d^n=(0.5)(D)\left(\frac{Sw^n}{d^n}\right)\left[C_1+K_m^n+\frac{f_n\cdot d^n\cdot J_d^m}{Sw^n\cdot D}-\sqrt{\left(C_1+K_m^n+\frac{f_n d^n\cdot J_d^m}{Sw^nD}\right)^2-4C_1\left(\frac{f_n\cdot d^n\cdot J_d^m}{Sw^n\cdot D}\right)}\right]. \tag{4}$$

Note that the + sign has been dropped [11], as this would imply a negative value for the solute concentration at the membrane.

A series of curves was then produced by substituting biologically relevant values for each of the variables in Eq. (4). These values of J_d at different values of C_1 were then plotted according to the Eadie-Hofstee derivation of the Michaelis-Menten equation. In this manner it is possible to illustrate the way in which variation in each variable influences the estimate of the magnitude of the kinetic constants K_m and J_d^m from the plot of J_d *vs.* J_d/C_1.

For many probe molecules active and passive transport proceed concurrently. The contribution of passive permeation is given by the product PC_2 where P is the passive permeability coefficient and C_2 is the concentration of the probe molecule at the aqueous-membrane interface. In the presence of an unstirred water layer the uptake of J_d due to passive permeation [10] is given by

$$P = \frac{J_d/S_m}{C_1 - \frac{J_d \cdot d}{DS_w}}. \tag{5}$$

Thus the total experimentally demonstrated uptake, J_d, for given values of C_1, d, S_w, d, D, K_m and J_d^m, can be calculated by Eqs. (4) and (5).

Results

1. Varying the Effective Resistance of the Unstirred Water Layer

When the effective resistance of the unstirred layer is zero, there is a linear relationship between J_d and J_d/C_1 (Fig. 1, Curve *A*). In this example, the slope is -1, which represents the assigned value of the K_m of 1 mM. As the resistance of the unstirred layer is increased, the relationship between J_d *vs.* J_d/C_1 deviates from the ideal linear relationship. The curvilinearity is produced regardless of the manner by which the magnitude of the resistance of the unstirred layer is increased: by increasing the effective thickness of the unstirred layer, by decreasing the effective surface area of the unstirred layer, or by decreasing the value of free diffusion coefficient. Since this relationship is curvilinear over a wide range of values of J_d/C_1, and therefore of C_1, it is not possible to identify a linear portion from which extrapolation of the *y*-axis would be possible. Therefore, this plot has little use in the identification of the maximal transport rate even when the resistance of the unstirred layer is low.

Using the Eadie-Hofstee plot, the magnitude of the Michaelis constant K_m is normally derived from the slope of J_d *vs.* J_d/C_1. Clearly this is not possible in the presence of an unstirred layer because of the curvilin-

earity of the relationship (Fig. 1). When the resistance of the unstirred layer is zero, $J_d = 1/2J_d^m$ when $C_2 = K_m$. As the resistance is varied, $J_d = 1/2J_d^m$ when J_d/C_1 approaches J_d/K_m. Thus an estimate of the magnitude of the deviation of the apparent affinity constant K_m^* from the true Michaelis constant K_m can be approximated from the difference between the value of (J_d/C_1) at $J_d = 1/2J_d^m$ when the effective resistance of the unstirred layer is zero, compared with the corresponding value of (J_d/C_1) at different magnitudes of unstirred layer resistance. These values of $(J_d/C_1) - (J_d/C_1)^*$ are derived from Fig. 1 and are shown in Fig. 2 as a function of the effective resistance of the unstirred layer. It must be stressed that since the relationship between J_d *vs.* J_d/C_1 is linear only under the special condition of zero unstirred layer resistance (curve *A*), the K_m cannot be estimated from this plot when UWL resistance is greater than zero. For this reason, the K_m^* of curves *B* to *H*, Fig. 1, cannot be determined. The value $(J_d/C_1) - (J_d/C_1)^*$ at $J_d/2$ simply reflects the deviation of the value of J_d/C_1 for curves *B* to *H* at $J_d^m/2$ from the value of J_d/C_1 for zero UWL resistance, and as such indirectly reflects the deviation between the true and apparent values of the Michaelis constant. When the resistance approaches zero (curve *A*), K_m^* equals K_m and the value of K_m can accurately be determined from the slope of the relationship between J_d *vs.* J_d/C_1. With increasing values of unstirred layer resistance the deviation between (J_d/C_1) and $(J_d/C_1)^*$ increases markedly. For a given change in the value of the resistance, the deviation is greater for lower rather than for higher magnitude of resistance. Thus, it would be anticipated that the experimental demonstration of variations in K_m^* under conditions selected to yield different values of unstirred layer resistance would be easier to demonstrate when the resistance was initially relatively low, rather than high. The failure of a given experimental manipulation to produce a change in K_m^* may be due to the presence of a very high unstirred layer resistance: the manipulation may have greatly reduced the resistance, but its magnitude may have remained sufficiently large so as to obscure the demonstration of changes in the apparent affinity constant K_m^*.

2. Varying the True Michaelis Constant, K_m

The theoretical relationship between J_d and J_d/C_1 in the presence of an unstirred layer of zero resistance is shown by the dotted line in Fig. 3. When the resistance of the unstirred layer is low, the K_m^* approaches K_m;

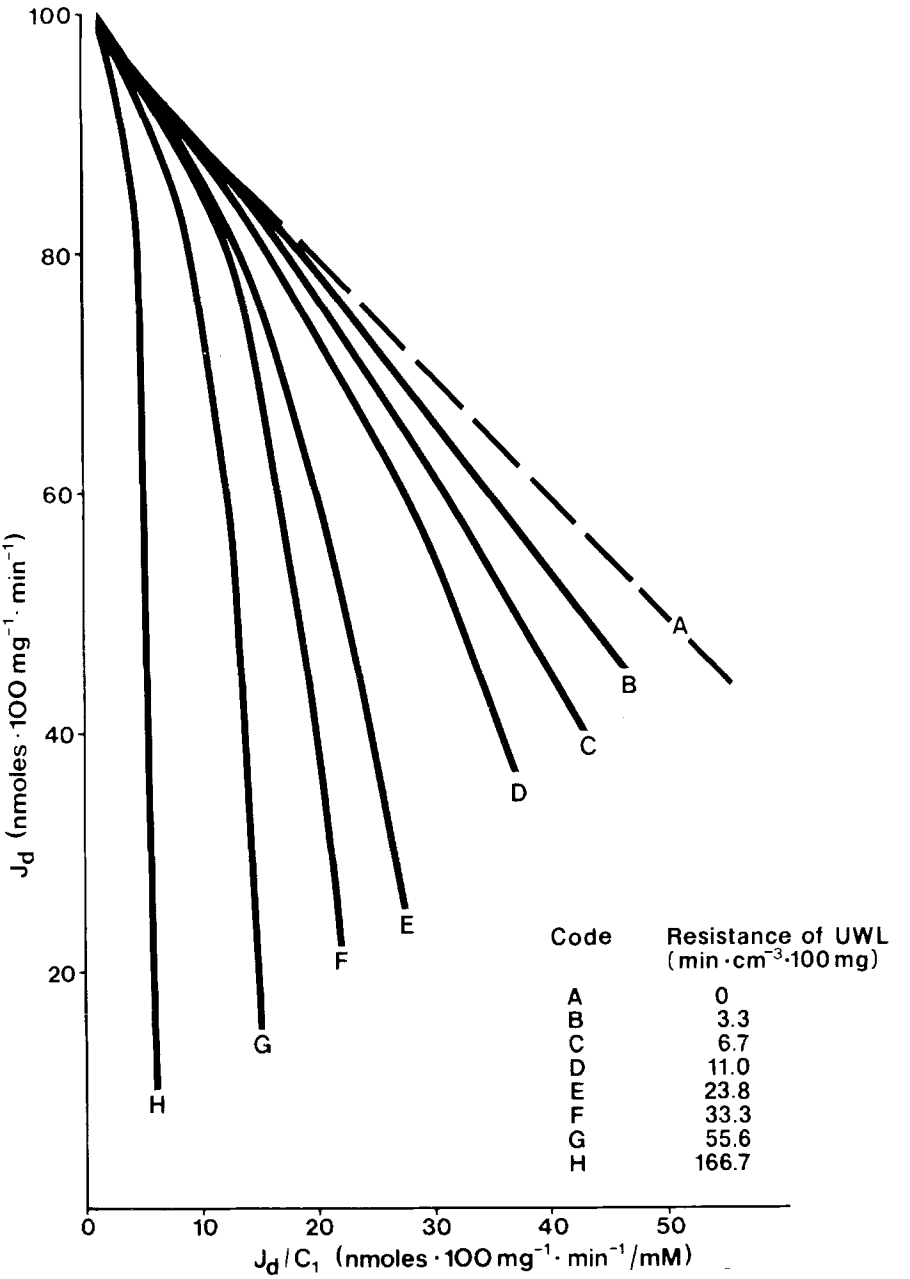

Fig. 1. Estimation of affinity constant (K_m) and maximal transport rate (J_d^m) from the relationship between J_d *vs.* J_d/C_1, derived from the Michaelis-Menten equation. J_d is the unidirectional flux rate, and C_1 is the concentration of the probe molecule in the bulk phase. Extrapolation of this linear relationship to the *y*-axis gives the value of the maximal transport rate, J_d^m, and extrapolation to the *x*-axis gives the value J_d^m/K_m, where K_m is the true Michaelis affinity constant. The slope has the negative value of $K_m(-K_m)$. The dotted line in this figure represents the relationship between J_d and J_d/C_1 when the effective resistance of the unstirred water layer is zero. This diagram illustrates the

for a given value of unstirred water resistance, there is less deviation between K_m and K_m^* when K_m is large than when small (Fig. 3*A*). In contrast, when the resistance of the unstirred layer is large, there is a greater deviation between K_m and K_m^* when K_m is larger.

3. Varying the Maximal Transport Rate, J_d^m

The theoretical relationship between J_d and J_d/C_1 in the presence of an unstirred layer of zero resistance is shown by the dotted line in Fig. 4. When the resistance of the unstirred layer is low, there is less deviation between K_m and K_m^* when J_d^m is low (Fig. 4*A*, Curves *C* and *D*), than when high (Curves *A* and *B*). When the resistance of the unstirred layer is high, there is gross deviation of the relationship between J_d *vs.* J_d/C_1 from linearity, and no approximation of J_d^m or K_m is possible (Fig. 4*B*).

4. Varying the Distribution of Transport Sites along the Villus, f_n

In the calculations thus far, the characteristics of the carrier have been assumed to be similar at each location along the villus and the resistance of the unstirred layer has been assumed to be similar at each locus. However, there is no experimental justification for this concept. Indeed, it is possible that the transport characteristics of the crypt cells differ from those near the villus tip. Therefore, the villus was arbitrarily divided into ten equal segments, and the characteristics of transport at each *n* site is varied, (Fig. 5); thus the rate of uptake and the dimensions of the unstirred water layer appropriate for the transport sites present in the ten equal segments have been designated as J_d^m, S_w^m, and d^m, respectively. When the resistance of the unstirred layer is low, there is little

manner in which the kinetics of carrier-mediated intestinal transport are altered by changes in the effective resistance of the unstirred water UWL layer from 3.3 to 166.7 $\text{min} \cdot 100\,\text{mg} \cdot \text{cm}^{-3}$; the different values for the resistance were obtained by changing the effective thickness of the UWL d from 1×10^{-2} to 10×10^{-2} cm, by varying the effective surface area of the UWL S_w from 1 to $10\,\text{cm}^3 \cdot 100\,\text{mg}^{-1}$, and by altering the free diffusion coefficient of the probe molecule D from 10×10^{-5} to $50 \times 10^{-5}\,\text{cm}^2\,\text{min}^{-1}$. In these calculations J_d^m was $100\,\text{nmol} \cdot 100\,\text{mg}^{-1} \cdot \text{min}^{-1}$, and K_m was 1 mM. These assigned values for J_d^m, K_m, d, S_w, D were substituted into a newly derived equation describing intestinal carrier-mediated transport in the presence of an unstirred water layer [2]

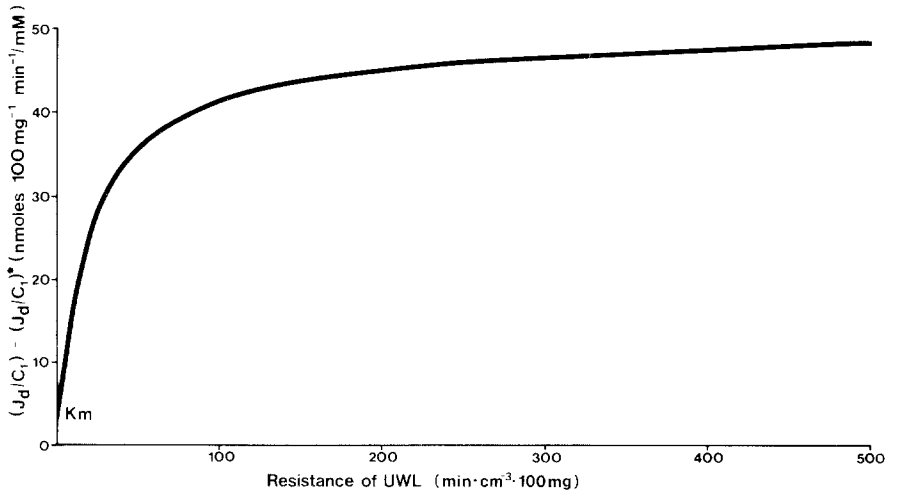

Fig. 2. Theoretical relationship between the effective resistance of the intestinal unstirred water layer (UWL) and the deviation between J_d/C_1, when the resistance of the unstirred layer was zero, from the value of J_d/C_1 at $J_d^m/2$ at different values of unstirred layer resistance. The effective resistance of the UWL was varied by altering the values of each variable (d, S_w and D), as described in the footnotes of Fig. 1. The K_m is estimated from the slope of the relationship between J_d *vs.* J_d/C_1. Thus, when $J_d = J_d^m/2$, $J_d/C_1 = J_d/K_m$. For example, in this diagram, $J_d^m = 100$ nmol · 100 mg^{-1} · min^{-1}, J_d at $J_d^m/2$ is 50 nmoles · 100 mg^{-1} · min^{-1}. When the resistance of the UWL was zero, the value of J_d/C_1 at $J_d = 50$ nmol · 100 mg^{-1} · min^{-1} was 50 nmol · 100 mg^{-1} · min^{-1}/mM; therefore the negative value of the slope was 1 mM, the assigned value of the true Michaelis constant. The value of J_d/C_1 at $J_d = J_d^m/2$ was arbitrarily chosen, and the deviation between the value of J_d/C_1 at $J_d^m/2$ at zero UWL resistance and J_d/C_1 at $J_d^m/2$ at the varying UWL resistances was plotted as a function of $d/S_w \cdot D$, the effective resistance of the UWL. Similar curves were obtained when different values of J_d were arbitrarily chosen, e.g., $J_d^m/3$, $J_d^m/4$, etc. As an additional example, when the resistance of the UWL was 55.6 min · 100 mg · cm^{-3} (Fig. 1, curve 6), J_d/C_1 at $J_d^m/2$ for UWL resistance of 55.6 min · 100 mg · cm^{-3} was 50 − 13 = 37 nmoles · 100 mg^{-1} · min^{-1}/mM. This value was then plotted as a function of $d/S_w \cdot D$. Note that initially small increases in the effective resistance of the UWL were associated with marked increases in the magnitude of the difference between the values of J_d/C_1 for zero unstirred layer resistance and the value of J_d/C_1 for curves drawn in the presence of an unstirred layer; but as the value of the UWL resistance increased further, there was relatively less change in the deviation between J_d/C_1 at zero UWL resistance, and J_d/C_1 at high values of resistance. In addition, half of the maximum deviation was achieved at an UWL resistance of only 20 min · 100 mg · cm^{-3}. It must be further stressed that, since the relationship between J_d *vs.* J_d/C_1 was curvilinear except under the special circumstance when UWL resistance was zero (Fig. 1), the multitude of K_m^*'s could not be accurately assessed from the relationship between J_d *vs.* J_d/C_1 in the presence of an unstirred water layer. The value $(J_d/C_1) - (J_d/C_1)^*$ is not equal to $K_m - K_m^*$, though it is related to it, and in this figure the value $(J_d/C_1) - (J_d/C_1)^*$ simply reflects the deviation of curves *B* to *H* in Fig. 1 from the value of J_d/C_1 at $J_d^m/2$ when UWL resistance is zero, as in curve *A*

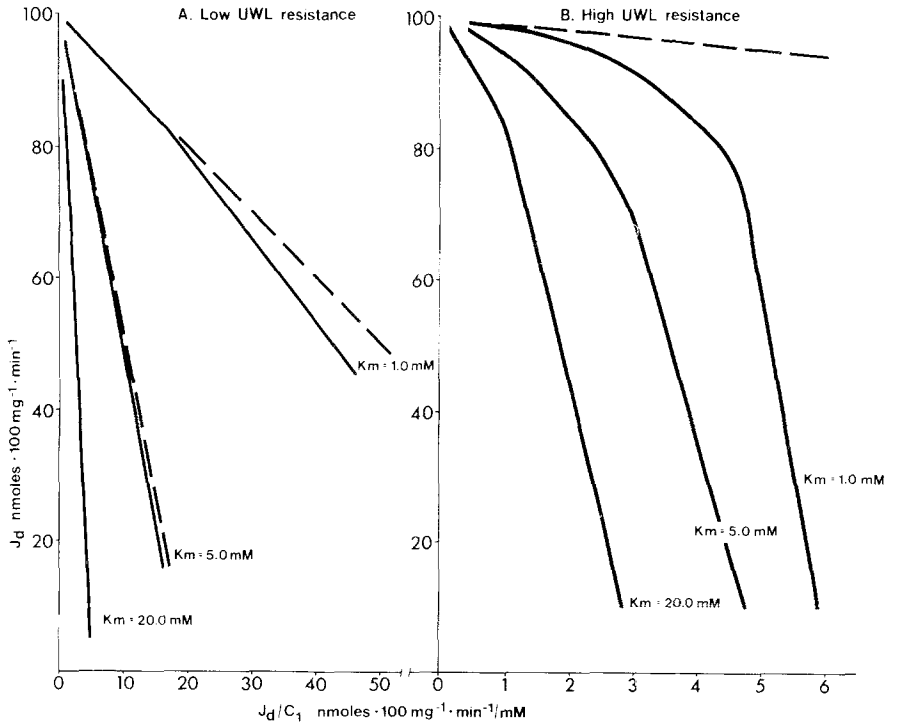

Fig. 3. Theoretical effect of varying the K_m on the K_m^* (apparent affinity constant) and the J_d^{m*} (apparent maximal transport rate), estimated from the relationship between J_d *vs.* J_d/C_1. This diagram illustrates the manner in which transport kinetics are altered by changes in the K_m of the transport carrier from 1 to 20 mM under condiitons where the resistance offered by the UWL was neither low or high. In these calculations J_d^m was 100 nmol 100 mg^{-1} · min^{-1} and D was 30×10^{-5} cm^2 min^{-1}. The dashed lines represent the relationship between J_d and J_d/C_1 when the effective resistance of the UWL was zero. In panel *B* only one dashed line is drawn: the scale of the *x*-axis in panel *B* is much less than in panel *A*, and the 3 separate dashed lines for $K_m = 1.0$ mM, $K_m = 5.0$ mM, and $K_m = 20.0$ mM very closely approximate the single line, as shown. When the effective resistance of the UWL was low (Panel *A*, 3.3 min · 100 mg · cm^{-3}), there was a close similarity between the true (K_m) and apparent (K_m^*) affinity constants, and the discrepancy between K_m and K_m^* was smaller when K_m was high (20 or 5 mM) than low (2 mM). When the effective resistance of the UWL was high (Panel *B*, 166.7 min · 100 mg · cm^{-3}), there was a curvilinear relationship between J_d and J_d/C_1; also note that there was a gross discrepancy between K_m and K_m^* and between J_d^m and J_d^{m*}, both when K_m was low and high

difference in the Eadie-Hofstee plot (Fig. 6*A*) when all transport occurs at one segment ($f_n = 1.0$, Curve *A*), as compared with 70% of the total maximal transport occurring at the first segment ($n = 1$), 20% from the second segment ($n = 2$), and 10%, the remaining, from the third segment ($n = 3$), as is shown in Curve *B*. The line of $f_n = 0.5$, 0.2, and 0.1×3 approaches the ideal line even more closely (Curve *C*), and the discrep-

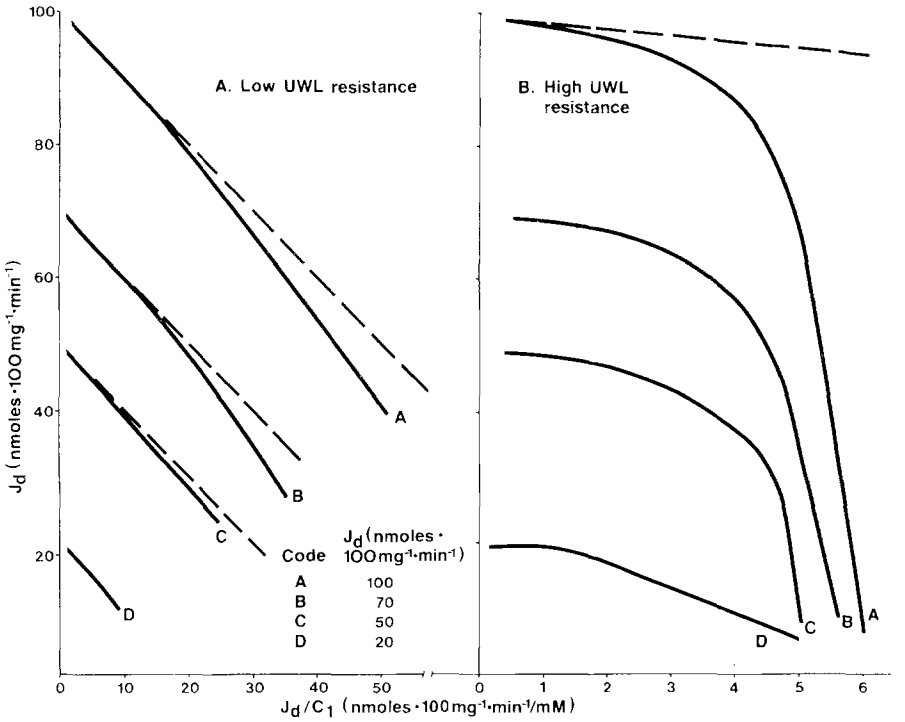

Fig. 4. Theoretical effect of varying the J_d^m on K_m^* and J_d^{m*} estimated from the relationship between J_d *vs.* J_d/C_1. This diagram illustrates the manner in which the apparent Michaelis constant and the apparent maximal transport rate are altered by changes in J_d^m from 10 to 100 nmol · 100 mg^{-1} · min^{-1}, under conditions where the resistance offered by the UWL was either low (3.3 · min · 100 mg · cm^{-3}) or high (166.7 min · 100 mg · cm^{-3}). In these calculations, K_m was 1 mM and D was 30×10^{-5} cm^2 · min^{-1}. The dashed lines represent the relationship between J_d and J_d/C_1 when the effective resistance of the UWL was zero. In panel *B* only, 1 dashed line is drawn; the scale of the *x*-axis in panel *B* is much less than in panel *A*, and the separate dashed lines for $J_d^m = 100$, 70, 50 and 20 very closely approximate the single line, as drawn. When the resistance of the UWL was low (panel *A*), there was only a small discrepancy between K_m and K_m^*, and this difference became less as the value of J_d^m declined. Similarly the discrepancy between J_d^{m*} and J_d^m was less for lower than for higher values of J_d^m (curves *C* and *D*, as contrasted with curves *A* and *B*). When the resistance of the UWL was high (panel *B*), there was a gross discrepancy between K_m and K_m^*, and J_d^m could not be estimated due to the curvilinear relationship between J_d and J_d/C_1

ancy between K_m and K_m^* increases further (Curve *D*) when the transport sites are evenly distributed along the villus ($f_n = 0.1 \times 10$). When the resistance of the unstirred layer is high (Fig. 6*B*), there is a curvilinear relationship between J_d and J_d/C_1, and once again neither J_d^m nor K_m can be estimated with any degree of confidence, regardless of the distribution of the transport sites along the villus.

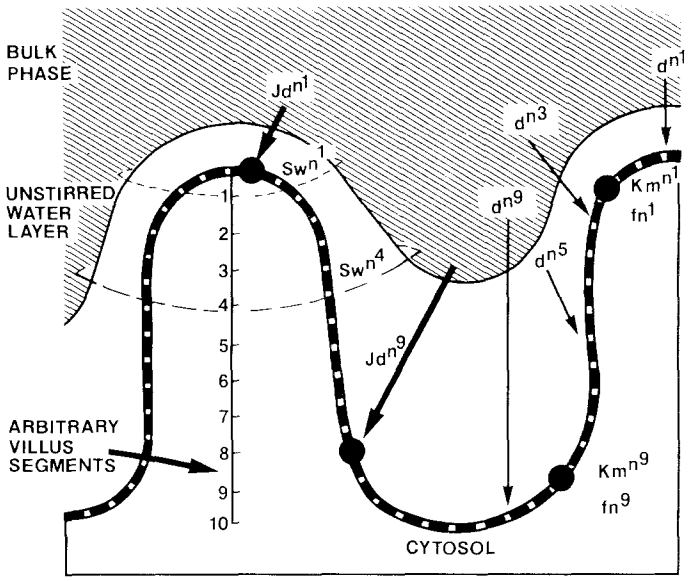

Fig. 5. Diagrammatic representation of the major barriers to active transport at different sites along the villus. The unstirred water layer can be assigned values for an effective thickness (d) and an effective surface are (S_w) so that the resistance of this layer to molecular diffusion is related to the ratio of d/S_wD. It is likely that the resistance of the unstirred water layer varies over transport sites present at different locations along the villus. For the mathematical presentation of this problem the villus was arbitrarily divided into 10 segments of equal height, and the rate of uptake and the dimensions of the unstirred water layer appropriate for the transport sites at each of these levels have been designated as J_d^m, S_w^m, and d^m, respectively

It has been shown experimentally that there is a "superficial" as well as a "deep" intestinal unstirred water layer [12]. When the effective resistance of the unstirred layer over each n site is increased, the anticipated result previously shown in Fig. 1 is observed; the relationship between J_d *vs.* J_d/C_1 becomes progressively more curvilinear and deviates markedly from the ideal linear relationship. This holds true for a variety of combinations of transport sites, from $f_n = 1.0$ *to* $f_n = 0.1 \times 10$. In sharp contrast, if the Michaelis constant varies at each site along the villus, and if the effective resistance of the unstirred layer over each n segment of the villus also varies, then the relationship between J_d *vs.* J_d/C_1 may be near-linear, curvilinear downwards or curvilinear upwards (Fig. 7*A–C*). Whereas many combinations of conditions will permit the demonstration of a downward curvilinear relationship (Figs. 1 and 3–5), the only circumstance under which this relationship becomes curvilinear upwards is when the transport sites are not concentrated at one site ($f_n \neq 1.0$) and

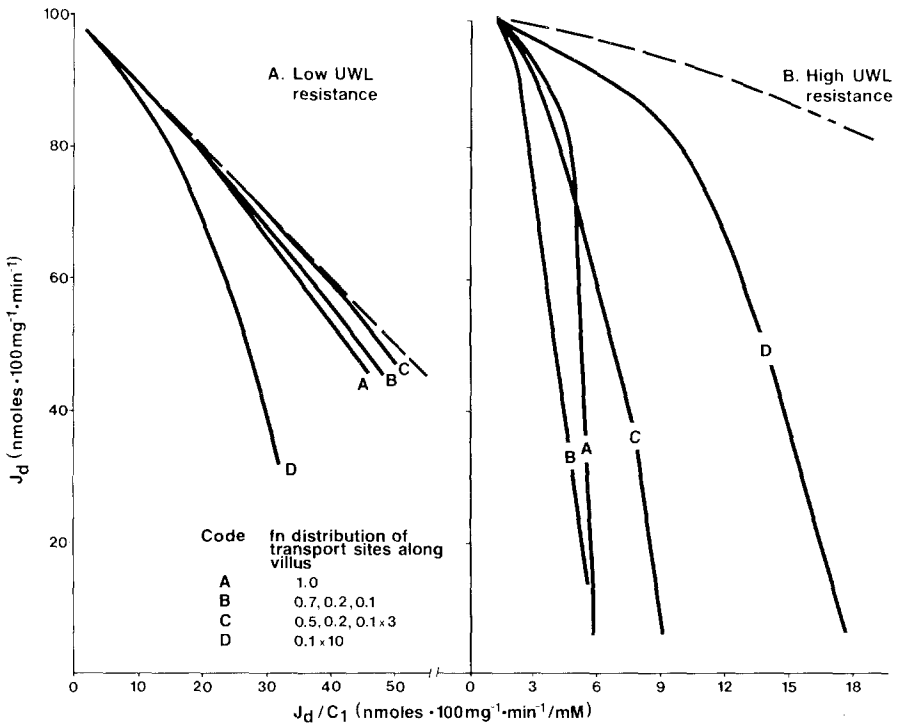

Fig. 6. Theoretical effect of varying the distribution of transport sites along the villus (f_n) on K_m^* and $J_d^{m}*$, estimated for the relationship between J_d *vs.* J_d/C_1. This diagram illustrates the manner in which carrier-mediated transport kinetics are altered by changes in f_n, with the K_m and effective resistance of the UWL over each carrier being similar. In panel *A* the effective resistance of the UWL was low (3.3 min · 100 mg · cm^{-3}) and in panel *B* the resistance was high (166.7 min · 100 mg · cm^{-3}). The dotted line represents the theoretical relationship between J_d and J_d/C_1 when the effective resistance of the UWL was zero. Curve *A* shows the kinetics of transport when all the transport carriers were in the first of ten equal villus segments ($f_{n1}=1.0$). In curve *B* 70% of the total active transport sites were located in the first segment ($f_{n1}-0.7$); 20% were in the second segment ($f_{n2}=0.2$), and 10% were in the third segment ($f_{n3}=0.1$). The total flux J_d is given by the sum of the individual fluxes contributed by each *n*th segment (J_d^n). In curve *C* 50% of the active transport sites were located in the first segment ($f_{n1}=0.5$), 20% in the second segment ($f_{n2}=0.2$) and 10% in the third, fourth, and fifth segments ($f_{n3}=0.1$, $f_{n4}=0.1$, $f_{n5}=0.1$) and the total flux was given by the sum of the fluxes occurring over these five segments. In curve *D*, 10% of the active transport sites were located in each of the ten segments ($f_{n1}=0.1$, $f_{n2}=0.1 \ldots f_{n10}=0.1$) and the total flux was obtained from the sum of the fluxes occurring over these ten segments. In these calculations J_d^m was 100 nmol · 100 mg^{-1} min^{-1}. Note that when the effective resistance of the UWL was low (panel *A*), changing the distribution of transport sites from the tip of the villus ($f_n=1.0$, curve *A*) to the upper half of the villus ($f_n=0.7$, 0.2, 0.1, curve *B*; and $f_n=0.5$, 0.2, 0.1 × 3, curve *C*), shifted the relationship between J_d *vs.* J_d/C_1 towards the theoretical line of zero UWL resistance (dotted line), but that the equal distribution of transport sites along the villus ($f_n=0.1 \times 10$, curve *D*) was associated with a further deviation away from the theoretical line. In contrast, when unstirred water layer resistance was high (panel *B*), relocating the carrier sites from the tip towards the base of the villus was initially associated with an increased (curve *B*) and then a decreased (curves *C* and *D*) deviation from the theoretical line

when both the effective resistance of the unstirred layer and the magnitude of the affinity constant vary at different positions along the villus. (Fig. 7*A*, curve *A*; Fig. 7*B*, curves *A* and *B*; Fig. 7*C*, curves *A*, *B* and *C*).

5. *The Effect of Passive Permeation on the Estimations of K_m and J_d^m when the Resistance of the Unstirred Layer is Varied*

Experimentally measured rates of unidirectional active flux are comprised of the contribution of both the carrier-mediated process as well as passive diffusion which proceeds concurrently, and failure to correct for the passive transport component leads to an over-estimation of the value of the Michaelis constant [17]. The next step therefore is to examine the effect of passive permeation on the estimates of K_m and J_d^m. The passive permeation coefficient of P of the probe molecule was arbitrarily assigned a value of $1\,\text{nmol}\cdot 100\,\text{mg}^{-1}\cdot\text{min}^{-1}\cdot\text{mM}^{-1}$, and the maximal transport rate J_d^m was assigned a value of $100\,\text{nmol}\cdot 100\,\text{mg}^{-1}\cdot\text{min}^{-1}$. The contribution of the passive component at any given concentration is given by the magnitude of P multiplied by C_2. The total experimentally determined flux rate J_d^T is given by the sum of the active plus the passive component; this was derived by adding the value of J_d from Eq. (4), and as shown in Figs. 1–4, 6 and 7. The total uptake J_d^T therefore represented the total of active plus passive transport. The value of P in the presence of an unstirred water layer has been shown to be given by Eq. (5).

$$P = \frac{J_d/S_m}{C_1 - \dfrac{J_d \cdot d}{DS_w}}.$$

Thus, arbitrary values were assigned for P, and the values of C_1, d, S_w and D were similar to those used in Eq. (4).

When the resistance of the unstirred layer is low (Fig. 8*A*), the relationship between J_d^T *vs.* J_d/C_1 changes from near-linear when P is zero, to curvilinear upwards when P is 1 nmol/100 mg/min/mM, (Fig. 8*A*, curve *B*). With greater values of P, the line becomes more sharply angulated upwards (Fig. 8*A*, curve *C*). When the resistance of the unstirred layer is high (Fig. 8*B*), the upward angulation becomes even more marked. Thus failure to correct for the contribution of the passive component precludes the approximation of the K_m and J_d^m from the Eadie-Hofstee plot. Furthermore, this upward deviation of the relationship between J_d *vs.* J_d/C_1 was apparent for a wide variety of values of K_m, J_d^m, f_n, as well as when f_n plus K_m were varied over the n villus segments.

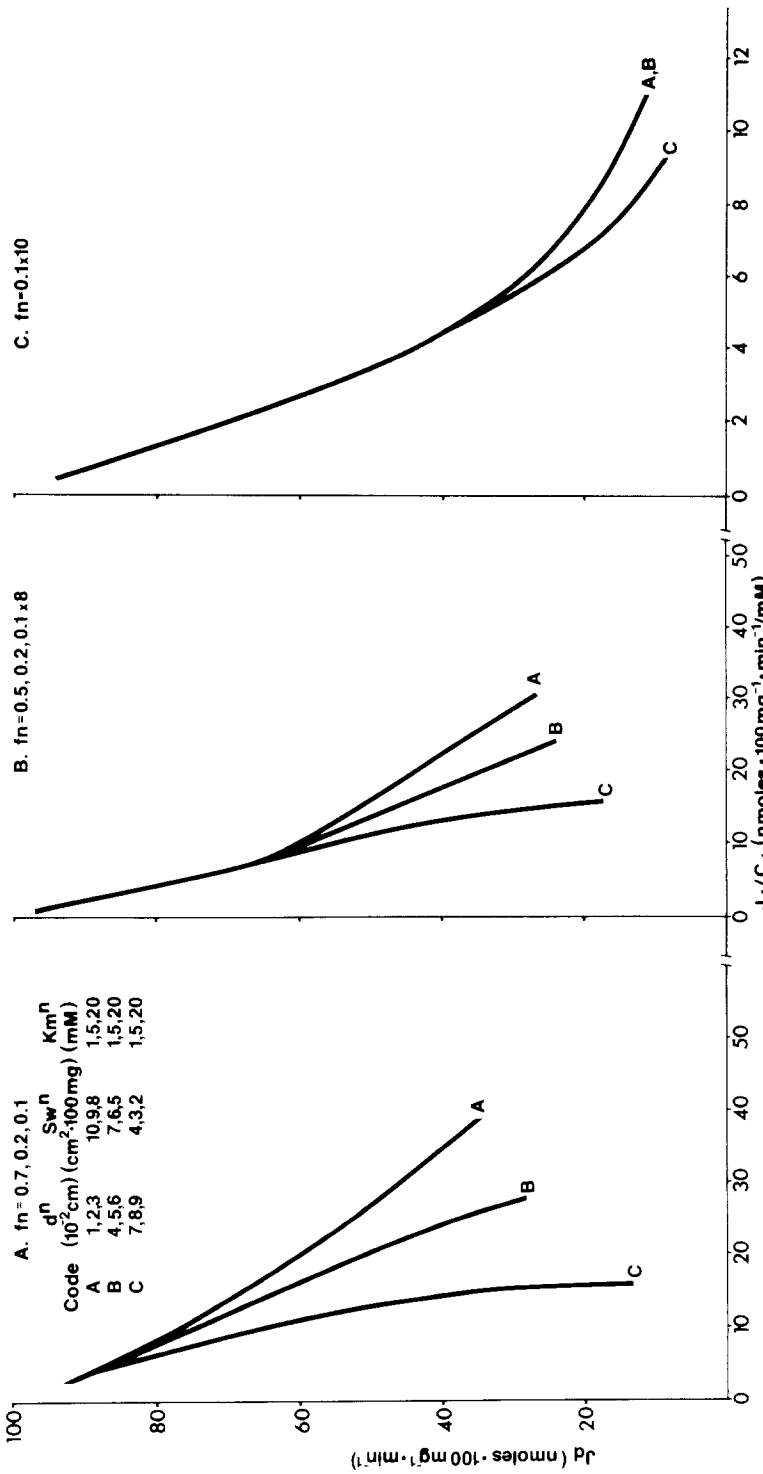
A. fn = 0.7, 0.2, 0.1
Code dn (10⁻²cm) Swn (cm²·100mg) Kmn (mM)
A 1,2,3 10,9,8 1,5,20
B 4,5,6 7,6,5 1,5,20
C 7,8,9 4,3,2 1,5,20
B. fn=0.5, 0.2, 0.1 x8
C. fn=0.1x10
Jd (nmoles · 100 mg⁻¹ · min⁻¹)
Jd/C1 (nmoles · 100 mg⁻¹ · min⁻¹/mM)
A,B

Discussion

Both quantitative and qualitative errors arise from the use of the Eadie-Hofstee plot to estimate the value of K_m and J_d^m. The necessary provision of a linear relationship between J_d vs. J_d/C_1 was apparent only under the following special circumstances:

a) low resistance of the unstirred layer (Fig. 1);

b) high numerical value of the Michaelis constant (Fig. 3*A*);

c) low maximal transport rate (Fig. 4*A*);

d) distribution of most of the carrier-mediated transport to the upper half of the villus (Figs. 6*A*, 7*A* and *B*);

e) correct adjustment for the contribution of the passive component (Fig. 8*A* and *B*).

Under these special circumstances the *y*-axis intercept gives a reasonable approximation of the J_d^m, and the slope yields an approximate value of the K_m. Under all other conditions, there is gross overestimation of the value of both J_d^m and K_m. However, the mere finding of such a linear relationship does not by itself provide any information as to the qualitative nature of the transport process. Fortunately the effective resistance

Fig. 7. Theoretical effect of varying the distribution of transport sites along the villus, the effective resistance offered by the UWL, and the K_m of the carriers in the different segments of the villus, on K_m^* and J_d^m*, estimated from the relationship between J_d *vs.* J_d/C_1. This diagram illustrates the manner in which the kinetics of active transport are affected by changes in f_n, K_m^n, d^n, and S_w^n. In contrast with Fig. 5, the value of both the K_m and the effective thickness and surface area of the UWL overlying the different villus segments was varied. In panel *A*, 70% of the total carrier transport sites were located in the first villus segment ($f_{n1}=0.7$); 20% were in the second segment ($f_{n2}=0.2$), and 10% were in the third segment ($f_{n3}=0.1$). In panel *B*, 50% of the transport sites were located in the first segment ($f_{n1}=0.5$), 20% in the second segment ($f_{n2}=0.2$), and 10% in the third, fourth, and fifth segments ($f_{n3}=0.1$, $f_{n4}=0.1$, $f_{n5}=0.1$). In panel *C*, 10% of the carrier transport sites were located in each of the ten segments ($f_{n1}=0.1, f_{n2}=0.1, \ldots, f_{n10}=0.1$) and the total flux was obtained from the sum of the fluxes occurring over each segment of the villus. In curve *A* of each panel, $K_m^{n1}=1$ mM, $K_m^{n2}=5$ mM, and $K_m^{n3\ldots10}=20$ mM; $d^{n1}=1\times10^{-2}$ cm, $d^{n2}=2\times10^{-2}$ cm and $d^{n3\ldots10}=3\times10^{-2}$ cm; $S_w^{n1}=10\,\text{cm}^2\cdot100\,\text{mg}^{-1}$, $S_w^{n2}=9$ and $S_w^{n3\ldots10}=8\,\text{cm}^2\cdot100\,\text{mg}^{-1}$. In curve *B* of each panel, $K_m^{n1}=1$ mM, $K_m^{n2}=5$ and $K_m^{n3\ldots10}=20$ mM; $d^{n1}=4\times10^{-2}$ cm, $d^{n2}=5\times10^{-2}$ and $d^{n3\ldots10}=6\times10^{-2}$ cm; $S_w^{n1}=7\,\text{cm}^2\cdot100\,\text{mg}^{-1}$, $S_w^{n2}=6$ and $S_w^{n3\ldots10}=5\,\text{cm}^2\cdot100\,\text{mg}^{-1}$. In curve *C* in each panel, $K_m^{n1}=1$ mM, $K_m^{n2}=5$ and $K_m^{n3\ldots10}=20$ mM; $d^{n1}=7\times10^{-2}$ cm, $d^{n2}=8\times10^{-2}$ cm and $d^{n3}=9\times10^{-2}$ cm; $S_w^{n1}=4\,\text{cm}^2\cdot100\,\text{mg}^{-1}$, $S_w^{n2}=3$ and $S_w^{n3\ldots10}=2\,\text{cm}^2\cdot100\,\text{mg}^{-1}$. In these calculations J_d^m was 100 nmol $\cdot$ 100 mg^{-1} $\cdot$ min^{-1}. Note that the relationship between J_d *vs.* J_d/C_1 was linear (panel *A*, curve *B*), curvilinear downwards (panel *A*, curves *B* and *C*; panel *B*, curve *C*), or curvilinear upwards (panel *B*, curves *A* and *B*; panel *C*, curves *A*–*C*), depending upon the value assigned to f_n, d^n and S_w^n

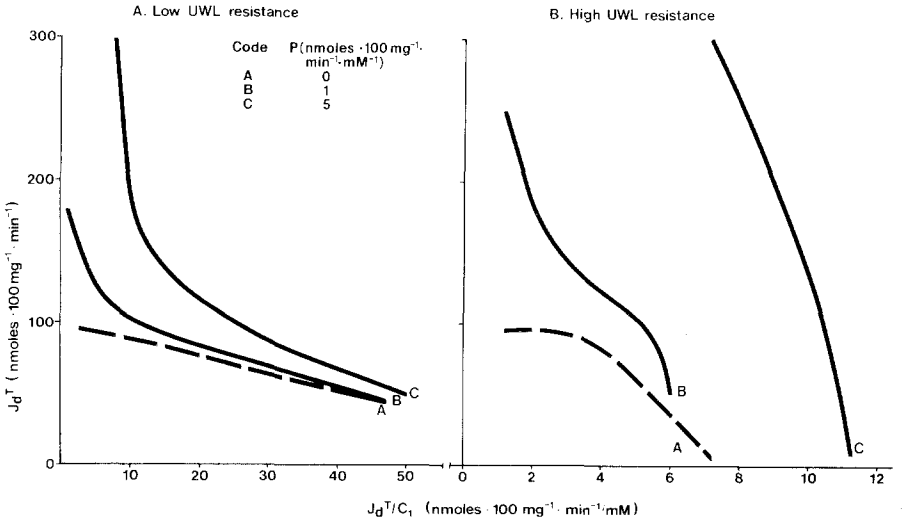

Fig. 8. Theoretical effect of varying the effective resistance of the UWL on the contribution of the passive component to the total unidirectional flux rate (J_d^T). This diagram illustrates the manner in which variations in the resistance of the UWL influence the contribution of passive permeation to the total flux rate. In panel *A* the resistance offered by the UWL was low (3.3 min · 100 mg · cm^{-3}), and in panel *B* the resistance was high (166.7 min · 100 mg · cm^{-3}). The passive permeability coefficient was varied from 1 to 5 nmol. 100 $mg^{-1} \cdot min^{-1}$ mM^{-1}; the Michaelis constant was 1.0 mM. In these calculations the maximal transport rate J_d^m was 100 nmol. 100 $mg^{-1} \cdot min^{-1}$, and *D* was 30×10^{-5} $cm^2 \cdot min^{-1}$. The total unidirectional flux J_d^T represents the sum of the contribution of the passive plus the carrier-mediated component. Note that even when the passive permeability coefficient *P* is as small as 1 nmol · 100 mg^{-1} · min^{-1} · mM^{-1} (curves *B*, panels *A* and *B*), there is a marked upward deviation of the *y*-axis intercept, an increase in the value of the *x*-axis intercept (J_d^m/K_m), and a rise in the value of the slope ($-K_m$). This deviation between the true and apparent values (K_m and K_m^*) of the Michaelis constant, and the true and apparent values (J_d^m and J_d^m*) of the maximal transport rate observed with failure to correct for the contribution of the passive component (as in Fig. 7) was also observed with varying the value of K_m from 1 to 20 mM, with varying the value of J_d^m from 10 to 100 nmol · 100 mg^{-1} · min^{-1}, and with varying the value of f_n from $f_n = 0.7, 0.2, 0.1$ to $f_n = 0.1 \times 10$

of the unstirred water layer can be varied experimentally [5, 12, 16]; if conditions are selected when this resistance is known to be low, it is possible to use this plot to estimate with a degree of precision the J_d^m and K_m. It must be emphasized, however, that the resistance of the unstirred layer must be known to be small, for indeed, a linear relationship between J_d and J_d/C_1 may also be seen over a wide range of values when the unstirred layer resistance is high (Figs. 1, 3*B*, 4*B* and 6*B*). A further consideration must be given to the potential limitations of an experimental situation designed to modify the resistance of the unstirred layer,

without in fact knowing the absolute values of the resistance. For example, the change in the effective resistance of the unstirred layer may be estimated from the change in the rate of absorption observed at two rates of intestinal perfusion [16]. However, if this change in resistance is such that either zero unstirred layer resistance is not approximated, or the resistance of the unstirred layer remains high, then there may in fact be little change in the relative discrepancy between the true and apparent values of K_m (Fig. 2), and the estimates of the magnitude of the kinetic constants will still be grossly in error.

If specific conditions are chosen when the resistance of the unstirred layer is known to be low, then the shape of the relationship between J_d *vs.* J_d/C_1 may provide useful information as to the characteristics of the membrane carriers at different sites along the villus. Assuming firstly that the appropriate corrections have been made for the passive component, then an upward deviation of the relationship between J_d vs. J_d/C_1 occurs only when the value of the true affinity constant varies at different sites along the villus, and when the resistance of the unstirred layers over each villus segment also varies (Fig. 7*A–C*). This relationship is never seen when just the distribution of the transport sites along the villus is changed (Fig. 6) or when the resistance of the unstirred layer overlying each villus segment is altered (Figs. 1, 3 and 4).

Experimentally observed uptake rates are determined by the contribution of both the carrier-mediated and passive processes. Even when the contribution of the passive component is small ($1\,\text{nmole} \cdot 100\,\text{mg}^{-1} \cdot \text{min}^{-1} \cdot \text{mM}^{-1}$), the estimate of J_d^m with the Eadie-Hofstee plot will be seriously jeopardized (Fig. 8); the magnitude of this error increases as the contribution of passive permeation increases. This limitation applies both when unstirred layer resistance is low and high (Fig. 8*A* and *B*). Thus, the finding of an upward curvilinear deviation from linearity of the relationship between J_d *vs.* J_d/C_1 suggests either that the value of the Michaelis constant plus the unstirred layer resistance vary at different sites along the villus (Fig. 7), or that there has been inadequate correction for the contribution of the passive component (Fig. 8).

The physiological significance of the intestinal unstirred water layer has been abundantly confirmed experimentally [1–9, 12–14, 16]; since it is now possible to experimentally vary the effective resistance of the UWL [4, 12], it will be possible to apply the principles elucidated in this theoretical consideration to determine whether there is indeed one or more monosaccharide active transport process in the intestine, whether

the kinetic constants of a given substrate truly vary at different sites along the intestine, and whether physiological events such as aging affect substrate transport by varying the resistance of the unstirred layer, or by varying the distribution of transport sites along the villus.

In summary, unless the resistance of the intestinal unstirred water layer is low, the use of the Eadie-Hofstee plot leads to serious errors in the estimation of the magnitude of both the maximal transport rate and the affinity constant. However, this plot may provide information on the characteristics and distribution of carriers present at different locations along the villus, and may also predict the adequacy of the correction for the contribution of passive permeation.

Abbreviations Used in the Text

C_1	Concentration of the probe molecule in the bulk phase
C_2	Concentration of the probe molecule at the aqueous-membrane interface
d	Effective thickness of UWL
D	Free diffusion coefficient
d^n	d at n th segment of the villus
f_n	Proportion of total carrier transport sites present on each segment of villus
J	Unidirectional flux of probe molecule, uncorrected for surface area
J_d	Unidirectional flux of probe molecule determined experimentally, corrected for surface area
J_d^m	Maximal transport rate, corrected for surface area
J_d^{m*}	Apparent maximal transport rate
J^m	Maximal transport rate, uncorrected for surface area
K_m	Michaelis constant (true affinity constant)
K_m^*	Apparent affinity constant
K_m^n	K_m at nth segment of the villus
n	The perpendicular height of the villus was divided into ten equal segments numbered n_1 to n_{10}
p	Passive permeability coefficient
S_m	Functional surface area of the membrane
S_w	Effective surface of UWL
S_w^n	S_w at nth segment of the villus
UWL	Intestinal unstirred water layer

This work was supported by a grant from the Medical Research Council. The secretarial assistance of Ms. Bonnie Oklek and Miss Laurie Bart is warmly acknowledged.

References

1. Dietschy, J.M. 1973. Mechanisms of bile acid and fatty acid absorption across the unstirred water layer and brush border of the intestine. *Helv. Med. Acta.* **37**:89
2. Dugas, M.C., Ramaswamy, K., Crane, R.K. 1975. An analysis of the D. glucose influx kinetics of *in vitro* hamster jejunum, based on considerations of the mass-transfer coefficient. *Biochim. Biophys. Acta* **382**:576

3. Hayumpa, M., Nichols, S., Schenker, S., Wilson, F.A. 1976. Thiamine transport in thiamine-deficient rats. Role of the unstirred water layer. *Biochim. Biophys. Acta* **436**:438
4. Lewis, L.D., Fordtran, J.S. 1975. Effect of perfusion rate on absorption, surface area, unstirred water layer thickness, permeability and intralumenal pressure in rat ileum *in vivo*. *Gastroenterology* **68**:1509
5. Lukie, B.E., Westergaard, H., Dietschy, J.M. 1974. Validation of a chamber that allows measurement of both tissue uptake rates and unstirred layer thickness in the intestine. *Gastroenterology* **67**:652
6. Read, N.W., Levin, R.J., Holdsworth, C.D. 1976. Electrogenic glucose absorption in untreated and treated coeliac disease. *Gut* **17**:444
7. Read, N.W., Barker, D.C., Levin, R.J., Holdsworth, C.D. 1977. Unstirred layer and kinetics of electrogenic glucose absorption in the human jejunum *in situ*. *Gut* **18**:865
8. Rey, F., Diullet, F., Schmitz, J., Rey, J. 1974. Influence of flow rate on the kinetics of the intestinal absorption of glucose and lysine in children. *Gastroenterology* **66**:79
9. Sallee, V.L., Dietschy, J.M. 1973. Determinants of intestinal mucosal uptake of short- and medium-chain fatty acids and alcohols. *J. Lipid Res.* **14**:475
10. Thomson, A.B.R. 1978. Intestinal absorption of lipids: Influence of the unstirred water layer and bile acid micelle. Disturbances in lipid and lipoprotein metabolism. *Am. Physiol. Soc.* p. 29
11. Thomson, A.B.R., Dietschy, J.M. 1977. Derivation of the equations that describe the effects of unstirred water layers on the kinetic parameters of active transport processes in the intestine. *J. Theor. Biol.* **64**:277
12. Westergaard, H., Dietschy, J.M. 1974. Delineation of the dimensions and permeability characteristics of the two major diffusion barriers to passive mucosal uptake in the rabbit intestine. *J. Clin. Invest.* **54**:718
13. Wilson, F.A., Dietschy, J.M. 1974. The intestinal unstirred layer: Its surface area and effect on active transport kinetics. *Biochim. Biophys. Acta* **363**:112
14. Wilson, F.A., Sallee, V.L., Dietschy, J.M. 1971. Unstirred water layers in intestine: Rate determinant of fatty acid absorption from micelle solutions. *Science* **174**:1031
15. Winne, D. 1973. Unstirred layer, source of biased Michaelis constant in membrane transport. *Biochim. Biophys. Acta* **298**:27
16. Winne, D. 1976. Unstirred layer thickness in perfused rat jejunum *in vivo*. *Experientia* **32**:1278
17. Winne, D. 1977. Correction of the apparent Michaelis constant, biased by an unstirred layer, if a passive transport component is present. *Biochim. Biophys. Acta* **464**:118